Geochemical Perspectives Letters

Resolving the chlorine isotope composition of Earth's depleted mantle

G. Segee-Wright, J.C. Lassiter, J.D. Barnes, A.-S. Bouvier

Supplementary Information

The Supplementary Information includes:

- IRMS Methods
- SIMS Procedure
- Filtering for Data Quality in Literature and Filtering All Samples for Shallow Assimilation
- Calculating the Distance from the DMM Endmember in Pb, Sr, Nd Multi-Isotope Space
- δ^{37}Cl Values of Terrestrial Reservoirs and the Calculation of the Bulk Silicate Earth δ^{37}Cl value
- Tables S-1 to S-3
- Figures S-1 to S-5
- Supplementary Information References

IRMS Method

Aliquots of MORB samples were coarsely crushed with an agate mortar and pestle. For each sample, between 0.06 and 3.5 grams of glass were picked under a binocular microscope. Glass separates with no visible sign of alteration were crushed to <250µm and sonicated five times in 18.2 MΩ water, then dried at 40 ºC for two days. The crushed glass was then mixed with 99.99 % pure vanadium pentoxide flux that had been previously heated to 600 ºC for 24 hours in a muffle furnace following the procedure of Segee-Wright *et al*. (2023) to drive off any volatile halogens. The mixed sample and flux were then added to a quartz tube for Cl extraction via pyrohydrolysis. The extraction and measurement of chlorine isotope ratios at UT Austin utilized the method outlined by Eggenkamp (1994) and Magenheim *et al*. (1994), as modified by Barnes and Sharp (2006) and Sharp *et al*. (2007). Chlorine was extracted from the samples via pyrohydrolysis (*e.g.*, Shimizu *et al*., 2015) into an aqueous solution. The Cl-bearing solution was reacted with $AgNO_3$ to precipitate AgCl, then reacted with CH_3I to form CH_3Cl. CH_3Cl was then purified of excess CH_3I in a gas chromatography column in a continuous He flow. The CH_3Cl isotope composition was then analysed on a ThermoElectron MAT 253. Data are reported in standard per mil notation versus standard mean ocean chloride (‰ *vs*. SMOC). Error of δ^{37}Cl values is <0.2 ‰ (1 SD) based on long-term reproducibility of seawater standard measurements and a serpentine internal standard.

Pyrohydrolysis Cl yields

The Cl contents of pyrohydrolysis solutions were measured using a Dionex ICS 2000 Ion Chromatograph (IC) at UT Austin. Three to six mL of each pyrohydrolysis solution was pipetted into IC sample vials, and 125 µL of each sample solution was injected into the IC. Calibration standards with 0.05, 0.1, 0.25, 0.5, 1, and 5 µg/mL Cl were used to determine the concentrations of unknowns. The Cl concentrations of the MORB glasses were calculated from the total volume of pyrohydrolysis solutions, the masses of fused samples, and the Cl concentrations of the solutions. Cl yields from pyrohydrolysis were assessed by fusing basaltic and andesitic reference materials (JB-2, AGV-1, AGV-2,

and JA-2). Reference material Cl yields are 77-96 % based on GeoReM preferred values (Table S-1; Fig. S-1a; Jochum *et al*., 2015) but are within error of 100 % yield based on the uncertainty in the Cl concentrations of the reference materials (Table S-1) Calculated Cl contents of the MORB glasses closely match previously published SIMS Cl concentrations (Fig. S-1b). Measurements of procedural water blanks and fused vanadium pentoxide flux demonstrated that the vanadium pentoxide flux contains ~0.15 µg/g Cl, whereas the 18.2 MΩ water contains <2 ng/mL Cl. Chlorine contributed from the blank ranges from 1.0-3.6 % of the total Cl in the solution.

Table S-1 Measured and accepted GeoReM preferred Cl concentrations in geologic reference materials

Reference Material	Type	Pyrohydrolysis Cl (ppm) ± 2 SE	GeoReM Cl (ppm) ± 2 SE	Cl yield (%)
JA-2	Andesite	12 ± 1	16 ± 11	77
AGV-2	Andesite	62 ± 6	68 ± 14	92
BHVO-2	Basalt	97 ± 10	107 ± 94	91
AGV-1	Andesite	111 ± 11	133 ± 82	83
JB-2	Basalt	278 ± 28	290 ± 12	96

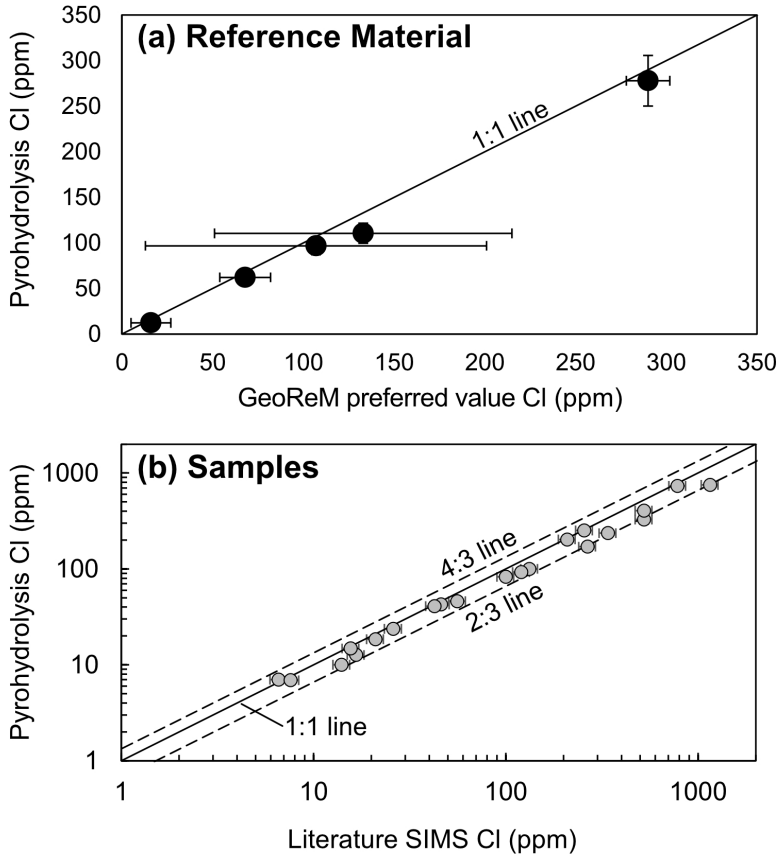

Figure S-1 (a) Comparison of GeoReM preferred Cl concentrations in reference materials and the Cl concentrations measured via pyrohydrolysis. **(b)** Comparison of previously published Cl concentrations collected via SIMS for MORB glasses and the Cl concentrations obtained via pyrohydrolysis of those same samples.

SIMS Procedure

Preparation of indium mounts for SIMS analyses

Indium mount preparation followed a procedure modified from Marshall *et al*. (2018). Glass chips with no visible alteration were picked from coarsely crushed samples. The chips were mounted on a glass slide in Crystalbond™ 509 and polished using successively finer diamond lap films with the final step using a <0.2-1 µm grit diamond polishing film. Polished glass chips were removed from the Crystalbond™ in two acetone baths, then cleaned in an ethanol bath followed by two 18.2 MΩ water baths. The chips were then heated at ~80 ºC for 20 minutes to drive off any residual water.

Indium mounts were composed of 1 inch diameter aluminium holders with an inner well with a 0.5-inch diameter with a small hole extending from the bottom of the well at the back of the mount. Aluminium holders were rinsed with ethanol and 18.2 MΩ water, then heated at 100 ºC for 20 minutes to drive off excess water. Ultrapure indium (99.999 % metal basis) was then added to the inner well of the holder and heated at ~250 ºC to melt the indium and volatilize any water or organic compounds introduced to the indium during storage or mount preparation. The mount was then cooled and the indium flattened by pressing the mount between two Melinex-covered polished aluminium plates in a table-top vise. Excess indium was removed with a clean steel pick from the hole in the back of the mount and removed from the edges of the holder with a razor blade. These steps were repeated until the indium was flush with the top of the aluminium holder and the indium had a mirror finish. Polished glass chips were then individually pressed into the surface of the indium with a glass slide. Once all chips were lightly pressed into the indium, the mount was then pressed between two Melinex-covered polished aluminium plates in a table-top vise. Excess indium was removed from the edges and back of the mount, and the mount was iteratively pressed again until the indium and glass chips formed a mirror-finished surface. The mount was then lightly polished by hand with 0.25 µm alumina grit on a polishing cloth, then lightly cleaned with ethanol and 18.2 MΩ water. The mount was then degassed in a vacuum chamber for two days and gold coated prior to analysis.

SIMS Measurements

Chlorine isotope ratios of the glasses were measured using a secondary ion mass spectrometer (SIMS) IMS 1280-HR at the University of Lausanne, Switzerland (UNIL). During analysis, the samples were sputtered with a 1.00 to 1.10 nA Cs^+ primary beam with an accelerating voltage of 10 kV. A presputtering was used at the beginning of each analysis with a 2nA primary beam, during which the beam was rastered over an area of 15 µm for 90 seconds to remove surface Cl contamination. Each analysis consists of 40 cycles of 6 seconds using a rastered beam over an area of 10 µm. This results in a total time per analysis of 7 minutes, including automated centring of the secondary beam in field and contrast apertures. Secondary ions were extracted into the mass spectrometer through a potential of 10 kV and through an energy slit set to a width of 50 eV, and secondary ions were counted on two electron multiplier (L2 and H2) detectors simultaneously with the count rate set at a maximum of $3x10^5$ counts per second to minimize electron multiplier aging effect. The entrance slit was set to 61 µm and multicollection exit slits 1 were used. Basaltic glass standards B2-1, B-20D (basalts; John *et al*., 2010) were used for calibration. Additionally, StH-G (andesitic glass; Jochum *et al*., 2006) was used to monitor the instrument stability and were place in each indium mount. Although no bulk $\delta^{37}Cl$ value exists for StH-G, it is available in larger quantity than B2-1 and B20-D and was proven to give reproducible data. StH-G had a typical reproducibility of 0.55 ‰ (2 SD).

Calibration of SIMS and IRMS Measurements

The $\delta^{37}Cl$ values of samples (n=6) analysed by both IRMS and SIMS largely fall along a 1:1 line and are within error of one another (Fig. S-2). However, SIMS $\delta^{37}Cl$ values are systematically lower than the IRMS values by an average of ~ 0.28 ‰. This offset is within the 2SD error of both the SIMS and IRMS methods. However, because this offset is systematic, it likely results from errors associated with the SIMS reference standard values that would be propagated to

the samples, not random error associated with sample measurements. Therefore, we correct for this offset for all SIMS measurements by adding 0.28 ‰ to the SIMS δ^{37}Cl measurements.

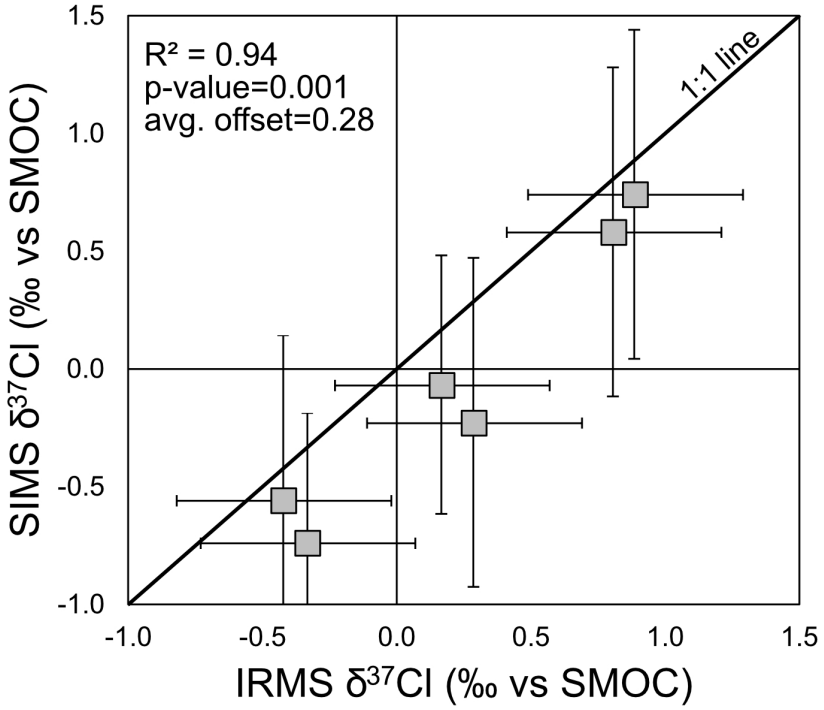

Figure S-2 Cl isotope ratios measured by IRMS vs Cl isotope ratios measured by SIMS in six MORB glasses from this study. SIMS measurements are systematically lower than the IRMS measurements by an average of 0.28 ‰. Error bars are external 2 SD of seawater standards (IRMS) or reference material (SIMS). R^2 and p-value are for a linear regression through the data.

Filtering for Data Quality in Literature and Filtering All Samples for Shallow Assimilation

Filtering Literature Data for Data Quality

Three previous Cl-isotope studies of MORB glasses have been recently published with a combined 36 samples analysed (Sharp *et al*., 2007; Bonifacie *et al*., 2008; Layne *et al*., 2009). Sharp *et al*. (2007) and Bonifacie *et al*. (2008) measured δ^{37}Cl values via IRMS methods and Layne *et al*. (2009) used a SIMS method. It is useful to combine the new data from this study with literature data, but care must be taken due to possible analytical artifacts in a subset of the analyses. Sharp *et al*. (2013) suggested that the low δ^{37}Cl values of MORB samples from Bonifacie *et al*. (2008) were the result of analytical artifacts due to measurement of small quantities of Cl. They found that the mass spectrometer will produce anomalously low δ^{37}Cl values when the quantity of Cl injected is too small (Sharp *et al*., 2013). However, this explanation can only be confidently applied to three samples because all but three samples from Bonifacie *et al*. (2008) were bracketed in measured Cl quantity by internal standard measurements (supplementary information in Bonifacie *et al*., 2008) and so are unlikely to have been affected by analytical artifacts related to sample size. However, these three samples from Bonifacie *et al*. (2008) had extremely small quantities of measured Cl (<125 µg Cl by dual inlet IRMS) that were not bracketed by standards and so may have been affected by these analytical artifacts. Therefore, we consider all data from Sharp *et al*. (2007) and Bonifacie *et al*. (2008) to be valid except the three extremely low-Cl samples.

Layne *et al*. (2009) measured $\delta^{37}Cl$ values of two MORB glasses via SIMS at the NORDSIMS facility, one from the Southwest Indian Ridge (SWIR) and one from the Mid-Atlantic Ridge (MAR). The SWIR and MAR glasses had Cl concentrations of 12 ppm and 50 ppm, respectively. These Cl concentrations are significantly lower than what is considered a quantifiable within reasonable error for $\delta^{37}Cl$ values using a comparable method at UNIL. Layne *et al*. (2009) measured each sample between 12 and 30 times to decrease the standard error of the mean $\delta^{37}Cl$ value. This may indeed produce the correct $\delta^{37}Cl$ value for the samples, but without the same method being performed on similarly low-Cl glasses with known $\delta^{37}Cl$ values, it is difficult to assess exactly how well this method worked. Therefore, we conservatively do not consider these $\delta^{37}Cl$ data in this study. Of the five total MORB glasses filtered overall, three of the five largely follow the same trends as the remaining data, but the two filtered samples with the lowest Cl contents (12 and 42 ppm) extend to extremely low $\delta^{37}Cl$ values and are not consistent with the remaining data.

In this study, we also do not include $\delta^{37}Cl$ values determined using the Pyrohydrolysis-Thermal Ionization Mass Spectrometry (P-TIMS) method of Magenheim *et al*. (1994, 1995). Subsequent studies have indicated that this method is subject to analytical artifacts resulting from trace quantity of sulphates or fluorides suppressing the Cs_2Cl^+ ionization and causing inconsistent $\delta^{37}Cl$ measurements (Stewart, 2000; Bonifacie *et al*., 2007, 2008; Sharp *et al*., 2007). Although the exact reason for the analytical error using the P-TIMS method may not be fully understood (Eggenkamp, 2025), there is enough doubt cast on the results to exclude them from discussion in this study.

Filtering for Potential Shallow Assimilation

Several previous studies have noted that shallow assimilation of seawater or brine can significantly increase the Cl content of MORB glasses. These studies have used a combination of Cl/K, Cl/Nb, and H_2O/Cl as filters for seawater and high salinity brine assimilation (*e.g.*, Michael and Cornell, 1998; Le Roux *et al*., 2006; Kendrick *et al*., 2013, 2017). Both Michael and Cornell (1998) and Shimizu *et al*. (2016) noted higher magmatic Cl/K in E-MORB than in N-MORB than in D-MORB. They attributed this to higher Cl/K in the enriched DMM source. Shimizu *et al*. (2016) suggested a threshold of Cl/K=0.1 for E-MORB, with any values greater than this potentially reflecting shallow assimilation. Based on this, we implemented different filtering criteria for E-MORB (Th/La≥0.0.07, $K_2O/TiO_2 \geq 0.15$), N-MORB ($0.035 > Th/La > 0.07$, $0.05 > K_2O/TiO_2 > 0.15$), and D-MORB ($Th/La \leq 0.035$, $K_2O/TiO_2 \leq 0.05$). When possible, we use Th/La as the filter because it is less likely to fractionate during partial melting (Shimizu *et al*., 2016). However, because many previously analysed samples do not have full suites of trace elements, we used K_2O/TiO_2 when Th/La was not available. Our filtering criteria were Cl/K<0.1 for E-MORB (Shimizu *et al*., 2016), Cl/K<0.06 for N-MORB, and Cl/K<0.03 for D-MORB. This is based on the data along the trend labelled "magmatic" in Figure 5b of Shimizu *et al*. (2016).

We note that filtering of a sample only indicates that it has *potentially* assimilated seawater/brine, not that it has done so. Studies have demonstrated that some MORB samples can have Cl/K greater than the thresholds used in this study, with primary mantle Cl/K of up to ~0.15 (Kendrick *et al*., 2017). For many samples above the threshold used in this study, it is ambiguous as to whether the Cl is derived from the mantle or shallow assimilation. Additional indices of assimilation not available in this study (e.g., Br, I, or B concentrations, or hydrogen or boron stable isotope ratios) would need to be measured to definitively determine if the samples had experienced significant assimilation.

Calculating the Distance from the DMM Endmember in Pb, Sr, Nd Multi-Isotope Space

Radiogenic isotope variability in the upper mantle is in part related to the incorporation of mantle endmember compositions likely genetically linked to deeply subducted lithosphere (*e.g.*, Stracke, 2012). These mantle endmembers are highly heterogenous, and so a single radiogenic isotope ratio will not increase the same amount with incorporation of different endmembers. For example, the HIMU mantle endmember has a $^{206}Pb/^{204}Pb$ significantly higher (>20.5) than DMM (17.5) but has a comparable $^{87}Sr/^{86}Sr$ (~0.7025), whereas EM-I endmember has a $^{206}Pb/^{204}Pb$ comparable to DMM

but has a significantly higher $^{87}Sr/^{86}Sr$ (~0.706) (Fig. S-3). Comparison of variations in $\delta^{37}Cl$ values to $^{206}Pb/^{204}Pb$ or $^{87}Sr/^{86}Sr$ will highlight HIMU and EM-I/II respectively (Fig. S-4a,b), but will obscure variations in other mantle components that may also have $\delta^{37}Cl$ variability.

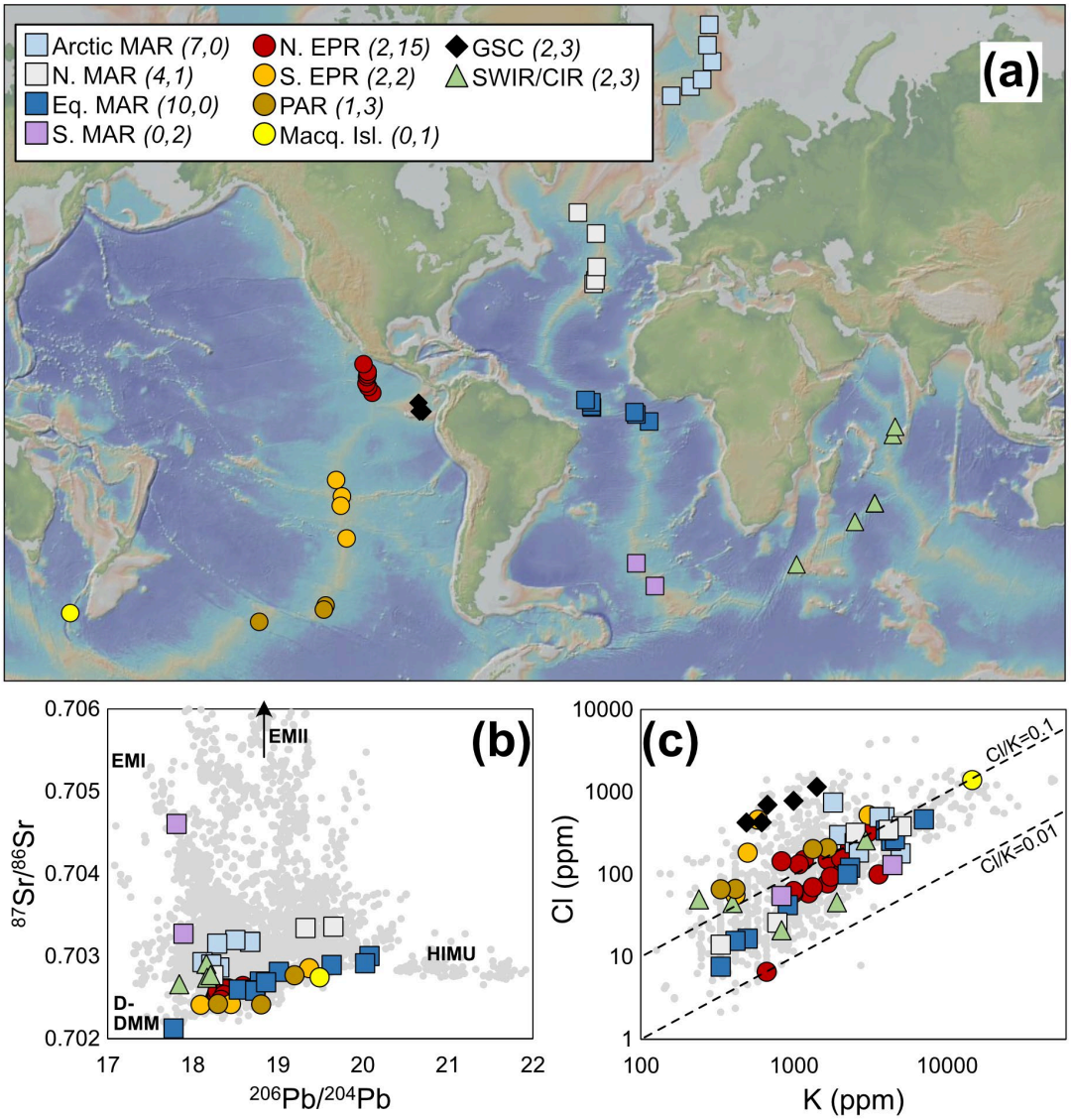

Figure S-3 (a) Map of the MORB sample locations from this study and from literature. Coloured symbols on the map denote different mid-ocean ridge (MOR) regions. Italic numbers in the legend are *(# of samples from this study, # from literature)*. **(b)** Previously published radiogenic Pb and Sr isotope data collected on the same MORB samples. Symbol colours are the same as in (a). Gray symbols are literature data from MORB and OIB from a compilation by Stracke (2012). **(c)** Potassium concentrations in the MORB glasses plotted against Cl concentrations. Symbols colours are the same as in (A). Gray symbols are MORB literature data from Shimizu *et al*. (2016), Kendrick *et al*. (2017), and Le Voyer *et al*. (2019). See Table S-3 for references to literature data. MAR=Mid-Atlantic Ridge; N. MAR=Northern MAR; Eq. MAR= Equatorial MAR; S. MAR=Southern MAR; EPR=East Pacific Rise; N. EPR=Northern EPR; S. EPR=Southern EPR; PAR=Pacific Antarctic Ridge; Macq. Isl.=Macquarie Island; GSC=Galapagos Spreading Centre; SWIR/CIR=Southwest Indian Ridge/ Central Indian Ridge.

To better determine the general effect of incorporation of subducted material in the mantle source of MORB, we calculate a distance parameter, defined as $D^{Pb/Sr/Nd}$ after the nomenclature from Jackson *et al*. (2014, 2020), in $^{206}Pb/^{204}Pb$, $^{87}Sr/^{86}Sr$, and $^{143}Nd/^{144}Nd$ isotope space for each sample. We calculated this as:

$$D^{Pb/Sr/Nd} = [(({}^{206}Pb/{}^{204}Pb_S - {}^{206}Pb/{}^{204}Pb_D)/X)^2 + (({}^{87}Sr/{}^{86}Sr_S - {}^{87}Sr/{}^{86}Sr_D)/Y)^2 + (({}^{143}Nd/{}^{144}Nd_S - {}^{143}Nd/{}^{144}Nd_D)/Z)^2]^{0.5} \quad \textbf{Eq. S-1}$$

The subscript S refers to glass samples and D refers to the radiogenic isotope composition of D-DMM from Workman and Hart (2005). X, Y, and Z represent the total range in MORB and OIB for $^{206}Pb/^{204}Pb$ (17.5-22), $^{87}Sr/^{86}Sr$ (0.70219-0.7186), and $^{143}Nd/^{144}Nd$ (0.123-0.51326), respectively (based on ranges used for the same procedure from Jackson *et al*., 2020). Normalizing the distance between a sample and DMM for a given isotope ratio to the total variability in global samples of that isotope ratio effectively scales the variations so that isotope ratios with the largest variability between endmembers are not weighted disproportionately. If this were not done, then $^{206}Pb/^{204}Pb$ would have a disproportionate weight relative to $^{87}Sr/^{86}Sr$ or $^{143}Nd/^{144}Nd$.

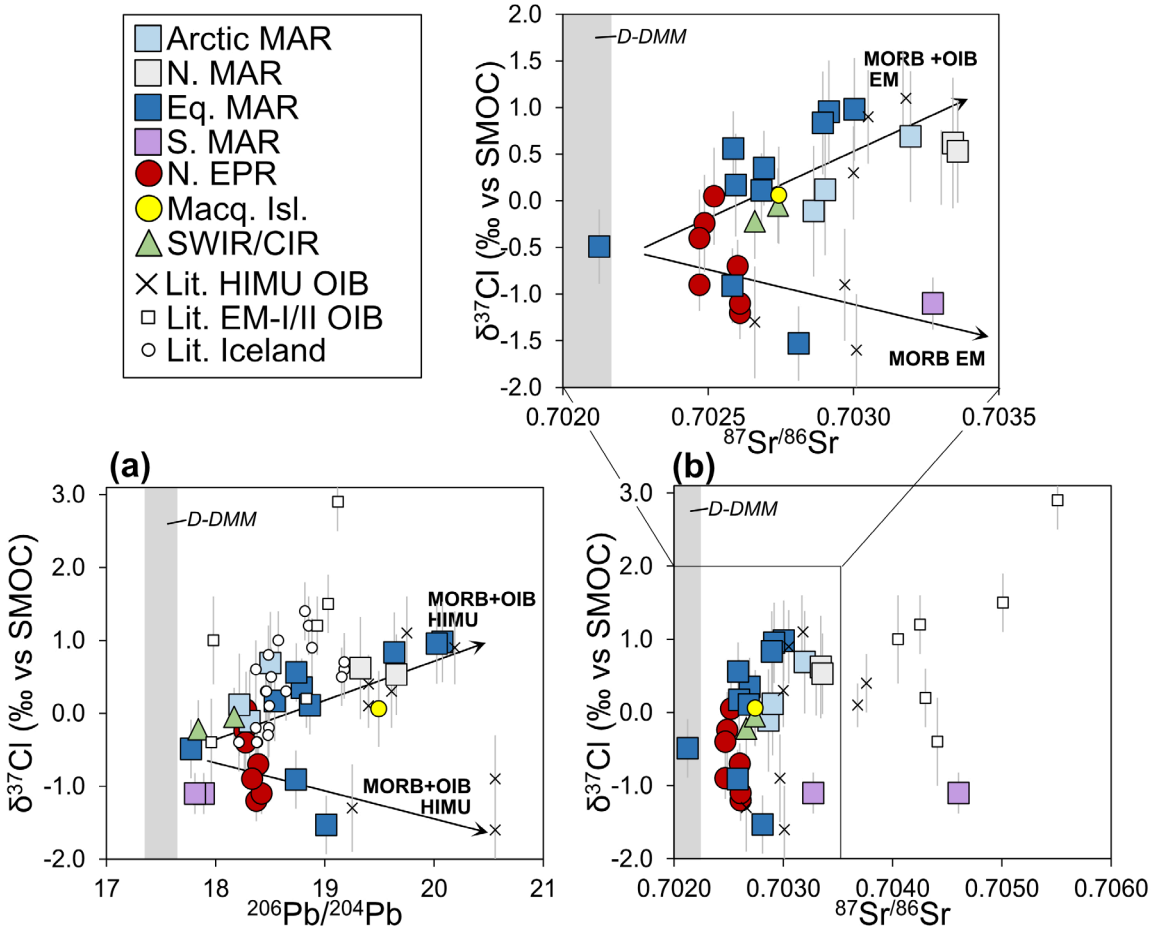

Figure S-4 Chlorine isotope ratios of MORB and OIB glasses from this study and literature plotted against **(a)** $^{206}Pb/^{204}Pb$ and **(b)** $^{87}Sr/^{86}Sr$. Error bars are 2 SD. Large coloured symbols are MORB samples from this study, Sharp *et al*., (2007) and Bonifacie *et al*. (2008). **(a)** Black arrows denote that HIMU-influenced MORB and OIB glasses extend to $\delta^{37}Cl$ values both lower and higher than DMM (see main text). **(b)** Black arrows denote that EM-I/II-influenced MORB glasses extend to $\delta^{37}Cl$ values both lower and higher than DMM, although OIB glasses only extend higher (see main text). Literature EM-I/II and HIMU OIB data are from John *et al*. (2010). Literature Iceland data are from Halldórsson *et al*. (2016). Gray vertical bars are the most depleted endmember DMM (D-DMM) for $^{206}Pb/^{204}Pb$ and $^{87}Sr/^{86}Sr$ values based on Workman and Hart (2005). References for $^{206}Pb/^{204}Pb$ and $^{87}Sr/^{86}Sr$ are given in Table S-3.

δ^{37}Cl Values of Terrestrial Reservoirs and the Calculation of the Bulk Silicate Earth δ^{37}Cl value

To calculate the Bulk Silicate Earth (BSE) δ^{37}Cl value, we conducted a procedure similar to the calculation of BSE Cl concentration in Kendrick *et al*. (2017). We used the Cl concentrations, δ^{37}Cl values, and masses of different surface reservoirs and the depleted mantle to calculate the δ^{37}Cl value of the BSE, assuming that all surface Cl originated in the mantle. The major Cl reservoirs at Earth's surface are seawater, evaporites, crustal brines, marine sediments, sedimentary rocks, and continental and oceanic crust. We used the Cl concentration and mass estimates from Kendrick *et al*. (2017) for each surface reservoir (Table S-2). Our estimates of the average δ^{37}Cl values of different reservoirs are based on the following:

Seawater: The δ^{37}Cl value of standard mean seawater is defined as 0.0 ‰, so no calculations are needed to determine the seawater δ^{37}Cl value.

Evaporites: We calculated the δ^{37}Cl value of evaporites as the average of Phanerozoic halite deposits (n=227) compiled in Barnes and Sharp (2017). The result is an average δ^{37}Cl value of -0.005 ± 0.05 ‰ (2 SE).

Crustal Brines: We calculated the δ^{37}Cl value of crustal brines as the weighted average of crustal brines (n=270) compiled in Barnes and Sharp (2017). Because brine salinity can vary dramatically (0.03-25.6 wt. % Cl; Barnes and Sharp, 2017), weighting the δ^{37}Cl values by the Cl concentration of the brines allows for a more accurate accounting of the overall δ^{37}Cl value of this reservoir. The result is an average δ^{37}Cl value of -0.25 ± 0.07 ‰ (2 SE).

Marine Sediments: The δ^{37}Cl value of marine sediments is calculated based on the weighted average of marine sediments (n=46) from Barnes *et al*. (2008, 2009) and Selverstone and Sharp (2015). The result is an average δ^{37}Cl value of -0.78 ± 0.21 ‰ (2 SE).

Sedimentary Rocks: There are very few Cl isotope analyses of global sedimentary rocks, especially considering the wide range of sediment types. To estimate the composition of sedimentary rocks, we took the weighted average of non-marine sediments (n=22) from Selverstone and Sharp (2015). There is large error associated with this estimate, but because sedimentary rocks make up a small fraction of the BSE Cl content (1-3 %; Table S-2), this has relatively little effect on the BSE δ^{37}Cl value. The result is an average δ^{37}Cl value of -0.05 ± 2.64 ‰ (2 SE).

Continental and Oceanic Crust: There are relatively few Cl isotope analyses of the altered oceanic crust (n=70; Bonifacie *et al.*, 2007; Barnes and Cisneros, 2012) and no analyses of material representative of continental crust as far as we are aware. For altered oceanic crust, the weighted average δ^{37}Cl value is 0.99 ± 0.28 ‰ (2 SE) for high-temperature altered oceanic crust (HT-AOC) and -0.17 ± 0.19 ‰ (2 SE) for low-temperature altered oceanic crust (LT-AOC). If we assume that oceanic crust has a thickness of 7,000 meters with the upper 2000 meters of LT-AOC with 26 ± 10 ppm Cl, 2000 meters of HT-AOC with 241 ± 96 ppm Cl, and 3000 meters of unaltered gabbro with 50 ppm Cl and an average δ^{37}Cl equivalent to the DMM (-0.5 ‰; This study) (Beaudoin *et al*., 2022), then the weighted average δ^{37}Cl value of the oceanic crust is +0.58 ± 0.91 ‰. We make the large assumption that alteration of the continental crust will result in approximately the same average δ^{37}Cl value as oceanic crust.

Depleted Upper Mantle: We used the updated estimate of the depleted mantle Cl concentration of 3 ± 1 ppm from Kendrick *et al*. (2024). We also made the same assumption as Kendrick *et al*. (2017) that 70 ± 20 % of the mantle has been depleted in Cl by melt extraction and degassing. Notably, the 3 ppm Cl estimate is based on a combination of MORB and OIB samples and so includes subducted heterogeneity in the estimate. The exact Cl content of deeply subducted lithosphere sampled by MORB and OIB is debated (*e.g.*, Lassiter *et al*., 2002; Hanyu *et al*., 2019). Because of this and because subduction-related samples extend to δ^{37}Cl values both higher and lower than the DMM estimate

(see main text), we make the large assumption that subducted materials do not perturb the overall mantle $\delta^{37}Cl$ value, which remains at the DMM estimate of −0.5 ‰. Additional work to better understand the $\delta^{37}Cl$ values, Cl contents, and quantity of different subducted material in the mantle will help to better constrain the bulk mantle $\delta^{37}Cl$ value. Therefore, we assume the bulk upper mantle has a $\delta^{37}Cl$ value of −0.5 ± 0.4‰.

Table S-2 Parameters used for BSE $\delta^{37}Cl$ value calculation

Reservoir	Mass (kg × 10^{21}) ± 2 SE	Fraction BSE Cl (%) ± 2 SE	Cl (ppm) ± 2 SE	$\delta^{37}Cl$ (‰) ± 2 SE
seawater	1.4 ± 0.07	27 ± 3	19,300 ± 970	0.00 ± 0.01
evaporites	0.03 ± 0.005	17 ± 2	550,000 ± 50,000	0.01 ± 0.05
marine sediments	0.5 ± 0.1	2 ± 1	4,000 ± 3,000	−0.78 ± 0.21
sedimentary rocks	1.5 ± 0.3	1 ± 0.3	700 ± 400	−0.05 ± 2.64
crustal brines	0.06 ± 0.03	6 ± 2	100,000 ± 50,000	−0.25 ± 0.07
cont+oc crust	26 ± 3	8 ± 2	300 ± 100	0.58 ± 0.91
processed mantle	2828 ± 808	9 ± 2	3 ± 1	−0.5 ± 0.4
calculated BSE	**4040**		**24 ± 3**	**−0.04 ± 0.13**

Using the Cl concentrations, $\delta^{37}Cl$ values, and masses of different reservoirs listed in Table S-2, we calculate the BSE $\delta^{37}Cl$ value as:

$$\delta^{37}Cl_{BSE} = [(\delta^{37}Cl_{seawater} \times X_{seawater}) + (\delta^{37}Cl_{crustal\text{-}brine} \times X_{crustal\text{-}brine}) + (\delta^{37}Cl_{evaporite} \times X_{evaporite}) + (\delta^{37}Cl_{marine\text{-}sediment} \times X_{marine\text{-}sediment}) + (\delta^{37}Cl_{sed\text{-}rx} \times X_{sed\text{-}rx}) + (\delta^{37}Cl_{cont\text{-}oc\text{-}crust} \times X_{cont\text{-}oc\text{-}crust})] / [([Cl]_{seawater} \times M_{seawater}) + ([Cl]_{crustal\text{-}brine} \times M_{crustal\text{-}brine}) + ([Cl]_{evaporite} \times M_{evaporite}) + ([Cl]_{marine\text{-}sediment} \times M_{marine\text{-}sediment}) + ([Cl]_{sed\text{-}rx} \times M_{sed\text{-}rx}) + ([Cl]_{cont\text{-}oc\text{-}crust} \times M_{cont\text{-}oc\text{-}crust})] \quad \textbf{Eq. S-2}$$

where

$$X_{reservoir} = ([Cl]_{reservoir} \times M_{reservoir}) / [([Cl]_{seawater} \times M_{seawater}) + ([Cl]_{crustal\text{-}brine} \times M_{crustal\text{-}brine}) + ([Cl]_{evaporite} \times M_{evaporite}) + ([Cl]_{marine\text{-}sediment} \times M_{marine\text{-}sediment}) + ([Cl]_{sed\text{-}rx} \times M_{sed\text{-}rx}) + ([Cl]_{cont\text{-}oc\text{-}crust} \times M_{cont\text{-}oc\text{-}crust})] \quad \textbf{Eq. S-3}$$

and $\delta^{37}Cl_{reservoir}$, $[Cl]_{reservoir}$, and $M_{reservoir}$ are the average Cl isotope ratios, the average Cl concentrations, and the masses of reservoirs from Table S-2, respectively.

To calculate the error propagated to the BSE $\delta^{37}Cl$ value from uncertainty in the $X_{reservoir}$ and $\delta^{37}Cl_{reservoir}$ values for each reservoir, we randomly sampled a number in a normal distribution around the mean of $X_{reservoir}$ and $\delta^{37}Cl_{reservoir}$ with a standard deviation equivalent to the 1 SE for both $X_{reservoir}$ and $\delta^{37}Cl_{reservoir}$ for all reservoirs in the above Eqs. S-2 and S-3. We then calculated the BSE $\delta^{37}Cl$ value using S-2 and S-3. We then performed this calculation 10,000 times for 10,000 random iterations. We then calculated the standard deviation of the 10,000 iterations of the BSE $\delta^{37}Cl$ value calculation. For each $X_{reservoir}$ and $\delta^{37}Cl_{reservoir}$, the iteratively calculated error is within 1 % of the algebraically calculated error (Fig. S-5). The result is a propagated 2 SE of the average BSE $\delta^{37}Cl$ value of ± 0.14 ‰ (Fig. S-5).

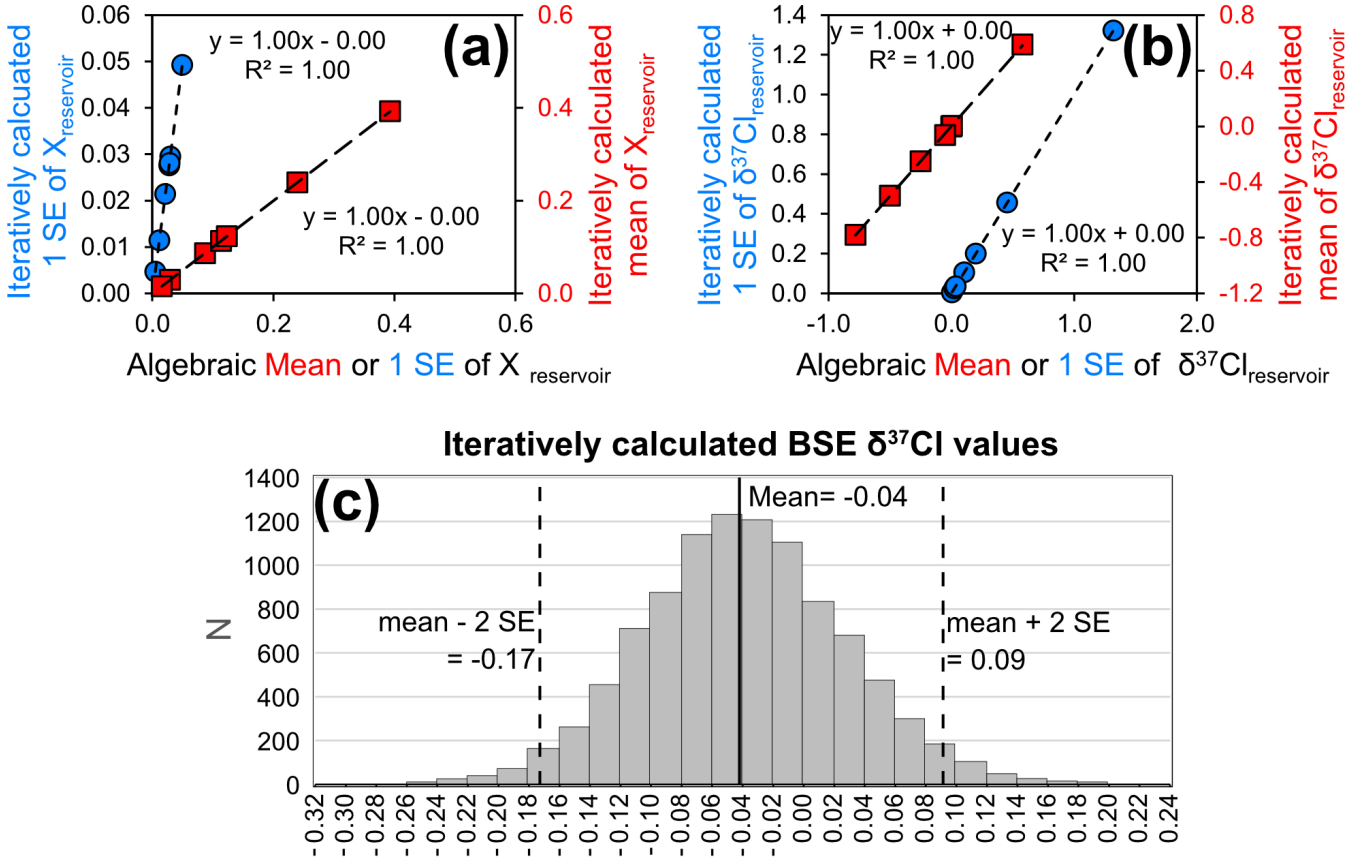

Figure S-5 (a-b) Comparison of the algebraically calculated mean (red) or standard error (1 SE; blue) with the iteratively calculated mean and standard error (see Supplementary Information S-5) for **(a)** $X_{reservoir}$ and **(b)** $\delta^{37}Cl_{reservoir}$ for reservoirs in Table S-2. All iteratively calculated values are equal within 1 % of the algebraically calculated values, supporting the robustness of the iterative calculation of the BSE standard error. **(c)** Histogram of the results of 10,000 calculations of the BSE $\delta^{37}Cl$ value.

Supplementary Data Table

Tables S-3 is available for download (.xlsx) from the online version of this article at http://doi.org/10.7185/geochemlet.2526 containing all Cl isotope data collected in this study and compiled by previous MORB and OIB studies, as well as previously published major, trace, and volatile element concentrations and radiogenic isotope ratios for these samples. The data in this table was compiled from 62 sources listed in Table S-3.

Supplementary Information References

Barnes, J.D., Sharp, Z.D. (2006) A chlorine isotope study of DSDP/ODP serpentinized ultramafic rocks: insights into the serpentinization process. *Chemical Geology* 228, 246–265. https://doi.org/10.1016/j.chemgeo.2005.10.011

Barnes, J.D., Sharp, Z.D. (2017) Chlorine Isotope Geochemistry. *Reviews in Mineralogy and Geochemistry* 82, 345–378. https://doi.org/10.1515/9783110545630-010

Barnes, J.D., Sharp, Z.D., Fischer, T.P. (2008) Chlorine isotope variations across the Izu- Bonin- Mariana arc. *Geology* 36, 883–886. https://doi.org/10.1130/G25182A.1

Barnes, J.D., Sharp, Z.D., Fischer, T.P., Hilton, D., Carr, M.J. (2009) Chlorine isotope variations along the Central American volcanic front and back arc. *Geochemistry Geophysics Geosystems* 10, Q11S17. https://doi.org/10.1029/2009GC002587

Barnes, J.D., Cisneros, M. (2012) Mineralogical control on the chlorine isotope composition of altered oceanic crust. *Chemical Geology* 326–327, 51–60. https://doi.org/10.1016/j.chemgeo.2012.07.022

Beaudoin, G.M., Barnes, J.D., John, T., Hoffmann, J.E., Chatterjee, R., Stockli, D.F. (2022) Global halogen flux of subducting oceanic crust. *Earth and Planetary Science Letters* 594, 117750. https://doi.org/10.1016/j.epsl.2022.117750

Bonifacie, M., Jendrzejewski, N., Agrinier, P., Coleman, M., Pineau, F., Javoy, M. (2007) Pyrohydrolysis-IRMS determination of silicate chlorine stable isotope compositions: Application to oceanic crust and meteorite samples. *Chemical Geology* 242, 187-201. https://doi.org/10.1016/j.chemgeo.2007.03.012

Bonifacie, M., Jendrzejewski, N., Agrinier, P., Humler, E., Coleman, M., Javoy, M. (2008) The chlorine isotope composition of Earth's mantle. *Science* 319, 1518–1520. https://doi.org/10.1126/science.1150988

Eggenkamp, H.G.M. (1994) *The geochemistry of chlorine isotopes*. Ph.D. Thesis, Universiteit Utrecht, 151.

Eggenkamp, H.G.M. (2025). *The Geochemistry of Stable Chlorine and Bromine Isotopes*. Second Edition, Advances in Isotope Geochemistry, Springer Nature, Cham, Switzerland. https://doi.org/10.1007/978-3-031-75633-7

Halldórsson, S.A., Barnes, J.D., Stefánsson, A., Hilton, D.R., Hauri, E.H., Marshall, E.W. (2016) Subducted lithosphere controls halogen enrichments in the Iceland mantle plume source. *Geology* 44, 679–682. https://doi.org/10.1130/G37924.1

Hanyu, T., Shimizu, K., Ushikubo, T., Kimura, J.-I., Chang, Q., Hamada, M., Ito, M., Iwamori, H., Ishikawa, T. (2019) Tiny droplets of ocean island basalts unveil Earth's deep chlorine cycle. *Nature Communications* 10, 60. https://doi.org/10.1038/s41467-018-07955-8

Jackson, M.G., Hart, S.R., Konter, J.G., Kurz, M.D., Blusztajn, J., Farley, K.A. (2014) Helium and lead isotopes reveal the geochemical geometry of the Samoan plume. *Nature* 514, 355-358. https://doi.org/10.1038/nature13794

Jackson, M.G., Blichert-Toft, J., Halldórsson, S.A., Mundl-Petermeier, A., Bizimis, M., Kurz, M.D., Price, A.A., Harðardóttir, S., Willhite, L.N., Breddam, K., Becker, T.W., Fischer, R.A. (2020) Ancient helium and tungsten isotopic signatures preserved in mantle domains least modified by crustal recycling. *Proceedings of the National Academy of Sciences* 202009663. https://doi.org/10.1073/pnas.2009663117

Jochum, K.P., Stoll, B., Herwig, K., Willbold, M., Hofmann, A.W., Amini, M., Aarburg, S., Abouchami, W., Hellebrand, E., Mocek, B., Raczek, I., Stracke, A., Alard, O., Bouman, C., Becker, S., Dücking, M., Brätz, H., Klemd, R., de Bruin, D., Canil, D., Cornell, D., de Hoog, C.-J., Dalpé, C., Danyushevsky, L., Eisenhauer, A., Gao, Y., Snow, J.E., Groschopf, N., Günther, D., Latkoczy, C., Guillong, M., Hauri, E.H., Höfer, H.E., Lahaye, Y., Horz, K., Jacob, D.E., Kasemann, S.A., Kent, A.J.R., Ludwig, T., Zack, T., Mason, P.R.D., Meixner, A., Rosner, M., Misawa, K., Nash, B.P., Pfänder, J., Premo, W.R., Sun, W.D., Tiepolo, M., Vannucci, R., Vennemann, T., Wayne, D., Woodhead, J.D. (2006) MPI-DING reference glasses for in situ microanalysis: New reference values for element concentrations and isotope ratios. *Geochemistry Geophysics Geosystems* 7, Q02008. https://doi.org/10.1029/2005GC001060

Jochum, K.P., Weis, U., Schwager, B., Stoll, B., Wilson, S.A., Haug, G.H., Andreae, M.O., Enzweiler, J. (2015) Reference values following ISO guidelines for frequently requested rock reference materials. *Geostandards and Geoanalytical Research* 40, 333–350. https://doi.org/10.1111/j.1751-908X.2015.00392.x

John, T., Layne, G.D., Haase, K.M., Barnes, J.D. (2010) Chlorine isotope evidence for crustal recycling into the Earth's mantle. *Earth and Planetary Sciences Letters* 298, 175–182. https://doi.org/10.1016/j.epsl.2010.07.039

Kendrick, M.A., Arculus, R., Burnard, P., Honda, M. (2013) Quantifying brine assimilation by submarine magmas: Examples from the Gala´pagos Spreading Centre and Lau Basin. *Geochimica et Cosmochimica Acta* 123, 150–165. https://doi.org/10.1016/j.gca.2013.09.012

Kendrick, M.A., Hémond, C., Kamenetsky, V.S., Danyushevsky, L., Devey, C.W., Rodermann, T., Jackson, M.G.,

Perfit, M.R. (2017) Seawater cycled throughout Earth's mantle in partially serpentinized lithosphere. *Nature Geosciences* 10, 222–227. https://doi.org/10.1038/ngeo2902

Kendrick, M.A. (2024) Halogen Cycling in the Solid Earth. *Annual Review of Earth and Planetary Sciences* 52, 7.1-7.26. https://doi.org/10.1146/annurev-earth-031621-111700

Lassiter, J.C., Hauri, E.H., Nikogosian, I.K., Barsczus, H.G. (2002) Chlorine-potassium variations in melt inclusions from Raivavae and Rapa, Austral Islands: constraints on chlorine recycling in the mantle and evidence for brine-induced melting of oceanic crust. *Earth and Planetary Science Letters* 202, 525–540. https://doi.org/10.1016/S0012-821X(02)00826-9

Layne, G.D., Kent, A.J.R., Bach, W. (2009) δ^{37}Cl systematics of a backarc spreading system: the Lau Basin. *Geology* 37, 427–430. https://doi.org/10.1130/G25520A.1

Le Roux, P.J., Shirey, S.B., Hauri, E.H., Perfit, M.R., Bender, J.F. (2006) The effects of variable sources, processes and contaminants on the composition of northern EPR MORB (8–10°N and 12–14°N): Evidence from volatiles (H_2O, CO_2, S) and halogens (F, Cl). *Earth and Planetary Science Letters* 251, 209-231. https://doi.org/10.1016/j.epsl.2006.09.012

Le Voyer, M., Hauri, E.H., Cottrell, E., Kelley, K.A., Salter, V.J.M., Langmuir, C.H., Hilton, D.R., Barry, P.H., Füri, E. (2019) Carbon Fluxes and Primary Magma CO2 Contents Along the Global Mid-Ocean Ridge System. *Geochemistry Geophysics Geosystems* 20. https://doi.org/10.1029/2018GC007630

Magenheim, A.J., Spivack, A.J., Volpe, C., Ransom, B. (1994) Precise determination of stable chlorine isotopic ratios in low-concentration natural samples. *Geochimica et Cosmochimica Acta* 58, 3117–3121. https://doi.org/10.1016/0016-7037(94)90183-X

Magenheim, A.J., Spivack, A.J., Michael, P.J., Gieskes, J.M. (1995) Chlorine stable isotope composition of the oceanic crust: implications for Earth's distribution of chlorine. *Earth and Planetary Science Letters* 131, 427-432. https://doi.org/10.1016/0012-821X(95)00017-7

Marshall, E., Lassiter, J.C., Barnes, J.D. (2018) On the (mis)behavior of water in the mantle: controls on nominally anhydrous mineral water contents in mantle peridotites. *Earth and Planetary Science Letters* 499, 219–229. https://doi.org/10.1016/j.epsl.2018.07.033

Michael, P.J., Cornell, W.C. (1998) Influence of spreading rate and magma supply on crystallization and assimilation beneath mid-ocean ridges: Evidence from chlorine and major element chemistry of mid-ocean ridge basalts. *Journal of Geophysical Research* 103, 18325-18356. https://doi.org/10.1029/98JB00791

Segee-Wright, G., Barnes, J.D., Lassiter, J.C., Holmes, D.J., Beaudoin, G.M., Chatterjee, R., Stockli, D.F., Hoffmann, J.E., John, T. (2023) Halogen enrichment in the North American lithospheric mantle from the dehydration of the Farallon plate. *Geochimica et Cosmochimica Acta* 348, 187–205. https://doi.org/10.1016/j.gca.2023.03.014

Selverstone, J., Sharp, Z.D. (2015) Chlorine isotope behavior during prograde metamorphism of sedimentary rocks. *Earth and Planetary Science Letters* 417, 120–131. https://doi.org/10.1016/j.epsl.2015.02.030

Sharp, Z.D., Barnes, J.D., Brearley, A.J., Chaussidon, M., Fischer, T.P., Kamenetsky, V.S. (2007) Chlorine isotope homogeneity of the mantle, crust, and carbonaceous chondrites. *Nature* 446, 1062–1065. https://doi.org/10.1038/nature05748

Sharp, Z.D., Mercer, J.A., Jones, R.H., Brearley, A.J., Selverstone, J., Bekker, A., Stachel, T. (2013) The chlorine isotope composition of chondrites and Earth. *Geochimica et Cosmochimica Acta* 107, 189–204. https://doi.org/10.1016/j.gca.2013.01.003

Shimizu, K., Suzuki, K., Saitoh, M., Konno, U., Kawagucci, S., Ueno, Y. (2015) Simultaneous determination of fluorine, chlorine, and sulfur in rock samples by ion chromatography combined with pyrohydrolysis. *Geochemical Journal* 49, 113-124. https://doi.org/10.2343/geochemj.2.0338

Shimizu, K., Saal, A.E., Myers, C.E., Nagle, A.N., Hauri, E.H., Forsyth, D.W., Kamenetsky, V.S., Niu, Y. (2016) Two-component mantle melting-mixing model for the generation of mid-ocean ridge basalts: Implications for the volatile content of the Pacific upper mantle. *Geochimica et Cosmochimica Acta* 176, 44–80. https://doi.org/10.1016/j.gca.2015.10.033

Stewart, M.A. (2000) *Geochemistry of dikes and lavas from Hess deep: implication for crustal construction processes beneath mid-oceanic ridges and the stable chlorine isotope geochemistry of mid-ocean ridge basalts*. PhD dissertation Thesis. Duke University, Durham, North Carolina.

Stracke, A. (2012) Earth's heterogeneous mantle: A product of convection-driven interaction between crust and mantle. *Chemical Geology* 330-331, 274-299. https://doi.org/10.1016/j.chemgeo.2012.08.007

Workman, R.K., Hart, S.R. (2005) Major and trace element composition of the depleted MORB mantle (DMM). *Earth and Planetary Science Letters* 231, 53-72. https://doi.org/10.1016/j.epsl.2004.12.005